Synthesis and Crystal structure of Cd-based metal-organic framework for removal of methyl-orange from aqueous solution

Article *in* Journal of Solid State Chemistry · July 2017

DOI: 10.1016/j.jssc.2017.07.019

CITATIONS
10

READS
821

4 authors, including:

Adedibu Clement Tella
University of Ilorin
89 PUBLICATIONS **472** CITATIONS

SEE PROFILE

Margaret Damilola Olawale
Elizade University
13 PUBLICATIONS **50** CITATIONS

SEE PROFILE

Joshua Obaleye
University of Ilorin
99 PUBLICATIONS **532** CITATIONS

SEE PROFILE

Journal of Solid State Chemistry 255 (2017) 157–166

Contents lists available at ScienceDirect

Journal of Solid State Chemistry

journal homepage: www.elsevier.com/locate/jssc

Synthesis and crystal structure of Cd-based metal-organic framework for removal of methyl-orange from aqueous solution

Adedibu C. Tella[a,*], Margaret D. Olawale[a,b], Markus Neuburger[c], Joshua A. Obaleye[a]

[a] Department of Chemistry, P.M.B.1515, University of Ilorin, Ilorin, Kwara State, Nigeria
[b] Department of Physical and Chemical Sciences, Elizade University, Ilara-Mokin, Ondo State, Nigeria
[c] University of Basel, Department of Chemistry, Spitalstrasse 51, Basel, Switzerland

ARTICLE INFO

Keywords:
MOFs
Adsorption
Methyl orange
X-ray crystallography

ABSTRACT

A novel $[Cd(INA)_2(H_2O)]$. ISB **(1)** (INA = isonicotinate; ISB = isobutanol) was synthesized through the reaction between the isonicotinic acid ligand and cadmium (II) salt and characterized by elemental analysis, FTIR and UV–Visible spectroscopies, SEM and Single crystal X-ray diffraction. The crystal is orthorhombic, space group *Pbca*, a = 12.24(10) Å, b = 15.4646(13) Å, c = 18.8445(17) Å, V = 3569(3) $Å^3$, Z = 8. The pentagonal bipyramid (seven coordinate) around the cadmium (II) ion is of the form CdN_2O_5 coordinating to four oxygen atoms from carboxylates, one oxygen atom from water molecule and two nitrogen atoms of pyridine. The structure of compound is stabilized by two hydrogen bonds namely intermolecular (O-H–O) and intramolecular type C-H–O accounting for polymeric nature of the metal-organic frameworks. **1** was studied for adsorptive removal of methyl orange (MO) from aqueous solution. Equilibrium isotherm study reveals that Langmuir model gave a better fitting result than the Freundlich model. The pseudo-second order model could be used to interpret adsorption kinetics. The maximum adsorption capacity calculated by Langmuir was 166 mg/g at 300 K. These results indicate the adsorption of MO on **1** is partly due to electrostatic interaction between methyl orange and the adsorbent. **1** could be used as adsorbent to remove methyl orange from aqueous solution.

1. Introduction

Metal organic frameworks being outstanding porous materials with exceptionally high surface area and tunable pore size [1–3] are of critical importance in diverse application such as gas storage and separation, adsorption, ion exchange, sensing, catalysis and drug delivery [3–13]. Recently, hazardous materials removal using MOF has been gaining ground due to the excellence characteristic of well-structured cavities, size and shape [14,15].

Construction of MOFs involves choosing of appropriate organic linker and inorganic metal. Also, the use of combination of organic ligands and nitrogen donor ligands has been proven to spawn interesting topology that aids adsorption [16]. Diverse synthetic methods have been employed in MOFs synthesis ranging from liquid-phase synthesis where separate metal salt and ligand solutions are agitated or solvent is added to a mixture of solid salt and ligand in a reaction vial, to mechano-synthesis involving milling or grinding the solid reactants for an efficient activation of reactant surface area [17]. Among the several synthetic methods includes mixing [18], refluxing [19], hydrothermal [20], solvothermal [21], microwave synthesis [22], sonochemistry [23], grinding [17], ball milling and liquid assisted milling [24]. In our recent studies, we reported that MOFs can be prepared by grinding and heating of solid reactants in absence of solvents [25,26].

Buildup of dyes in wastewater from industries such as textiles, paper, cosmetics, rubber, and plastics has been regarded as a substantial source of water pollution. Textile industries consume over 700,000 t of dyes annually and use up to 1 l of water per kg of dye processed and are third largest polluters in the world. Reactive dyes, an anionic dye, are most commonly used due to their provision of bright colors, excellent color fastness, and easy application [27]. However, many reactive dyes are toxic, carcinogenic and teratogenic to organisms and may cause direct harm to aquatic life such as mutation, lung cancer and neurological disorder. As the dyes are structurally complex, are of synthetic origin, and have high water solubility, their removal from effluent by the use of conventional physico-chemical and biological processes is difficult [28]. However, it has been reported that the adsorption technique provides a potential for the removal of dyes from aqueous solutions [29].

MOFs have been proven to be highly ordered structure like zeolite [30,31] and effective adsorptive materials due to the properties they

* Corresponding author.
E-mail address: ac_tella@yahoo.co.uk (A.C. Tella).

http://dx.doi.org/10.1016/j.jssc.2017.07.019
Received 7 April 2017; Received in revised form 8 July 2017; Accepted 16 July 2017
Available online 21 July 2017

possess i.e. large pores and surface area which make them better than the existing adsorbents. In order to contribute further towards synthesis and application of MOFs in environmental remediation [32,33], we hereby report the first crystal structure of cadmium isonicotinate MOF containing isobutanol as counter ion and its adsorptive ability for the removal of methyl orange from aqueous solution.

2. Experimental

2.1. Materials and physical measurements

All materials and solvents were purchased from Sigma Aldrich Company and used without purification. Melting points were measured on a WRS-1B digital melting point apparatus. The elemental analyses were performed on a Perkin-Elmer CHN Analyzer 2400 series II. The IR spectra were recorded on SHIMADZU scientific model FTIR 8400s Spectrophometer. Powder XRD analysis were measured on a Bruker D8 Advance X-ray diffractometer operating in a Da Vinci geometry equipped with Lynxeye detector using a CuKα-radiation (λ = 1.5406 Å). X-rays were generated by an accelerating voltage of 30 kV and a current flow of 40 mA. A receiving slit of 0.6 mm and a primary secondary slits of 2.5 mm were used. Samples were placed on a zero background sample holder and scanned over a range of 4–40° with a step size of 0.01° s^{-1}. Nitrogen adsorption measurements were performed on Quanta chrome (ASIQM) instrument. The total surface area was determined using Branauer-Emmett-Teller (BET) method. Pore size distribution was calculated by the Barrett-Joyner-Halenda (BJH) method.

Thermogravimetric analyses (TGA) were recorded with a TA instrument (TA-Q500). The sample weight was approximately1–2 mg and a heating rate of 10 °C min^{-1} under a nitrogen gas flow of 50 ml min^{-1} was used. X-ray Crystallographic analysis of the MOFs was carried out using a Bruker-Nonius KappaAPEX diffractometer equipped with an Incoatec mu micro focus X-ray source with Cu-anode. Direct method was used in solving the structure and F^2 was refined against all reflections. Structural solution and refinement were proficient using SIR97 and SHELXL97 [34].

2.2. Synthesis of $[Cd(INA)_2(H_2O)]$.ISB

Compound **1** was synthesized by mixing a solution of isonicotinic acid (0.123 g, 1 mmol) in isobutanol (10 ml) and solution of cadmium acetate dihydrate $[Cd(CH_3CO_2)_2{\cdot}2H_2O]$ (0.2 g, 0.5 mmol) in methanol (10 ml). Few drops of triethylamine were added. The mixed solution was refluxed at 200 °C for 30 min under 1000 revolution per minute (rpm). A clear solution was obtained and left standing for slow evaporation at room temperature. Colorless crystals were formed after 14 days. The crystals formed were separated out by filtration and washed with methanol and dried at room temperature in a desiccator (Scheme 1).

The equation of reaction is shown below:

Yield 78%, Mol. Wt. = 445.72 g/mol, Melting pt. = 286 °C, elemental analysis for $[CdC_{12}H_{10}N_2O_5].C_4H_7O$: calc. (found) C, 43.05 (43.31); H, 3.82 (3.81); N, 6.23 (6.28). IR (KBr, cm^{-1}): 3351–3218, 1742, 1546, 1381, 1014, 527, 441.

2.3. Adsorption experiment

The method described by Lin et al. [35], Haque et al. [14,15] was used. Batch equilibrium technique was used to study adsorption of methyl orange on $[Cd(INA)_2(H_2O)]$.ISB. An aqueous stock solution of methyl orange (200 ppm) was prepared by dissolving 200 mg of methyl orange in 1 l of deionized water. Aqueous dye solutions with different concentrations of the methyl orange (5–30 ppm) were prepared by successive dilution of the stock solution with deionized water. The concentration of methyl orange was determined using the absorbance (at λ_{MAX} = 465 nm) of the solutions after getting the UV spectra of the solution with a spectrophotometer (SHIMADZU UV-1650pc UV-vis spectrophotometer). The calibration curve was obtained from the spectra of the standard solutions (5–30 ppm) at a pH of 6.7.

Before adsorption, the compound 1 was activated by drying for 2 h under oven at 140 °C and kept in a desiccator. The compound after activation was named **1d**. Thermogravimetric analysis of **1d** was carried out to confirm that the MOF was fully activated and devoid of guest molecule (isobutanol). An exact amount of the adsorbents (**1d**) (0.01 g) were put into the aqueous solutions (30 ml) with the fixed dye concentration from 5 ppm to 30 ppm. The aqueous methyl orange solutions containing adsorbents (MOF) were mixed well with an orbital shaker at 200 revolution per minute (rpm) and were maintained for a fixed time (10–300 min) at 25 °C. After adsorption for a pre-determined time, the solutions were separated from adsorbent (MOF) using syringe filter, and the dye concentration was measured using UV–vis spectrophotometer. The amount of methyl red adsorbed onto MOF was calculated by mass-balance relationship.

$$Q_e = \frac{(C_o - C_e)v}{W}$$

C_0 and C_e (mg/L) are the liquid-phase concentrations of the methyl orange at time = 0 and t, respectively. V (L) and W (g) are the volume of the solution and the weight (g) of the adsorbents.

3. Results and discussion

The melting point determination of **1** (288 °C) and its ligand (255 °C) clearly are different from one another. The crystal is colorless and clearly different from the starting reactant. The Infrared spectrum of **1** is different from its ligand, which also suggests coordination of the ligand to the metal. The molecular weight of **1** show clear difference compared to the weights of the starting reactants. The elemental analyses for C, H, N were also consistent with the formula unit of the product, in comparison with its theoretically calculated values.

3.1. Infrared Spectroscopy

The infrared spectra of **1** have been studied in the 4000–400 cm^{-1} region (Fig. 1). Comparison of FT-IR spectra of **1** with that of isonicotinic acid revealed that the spectra are different indicating formation of new compound. The selected FT-IR absorption band (cm^{-1}) of isonicotinic acid and **1** are shown in Table S1. The IR spectroscopy data of the isonicotinic acid and 1 confirmed the coordination of the isonicotinic ligand to the cadmium ion through

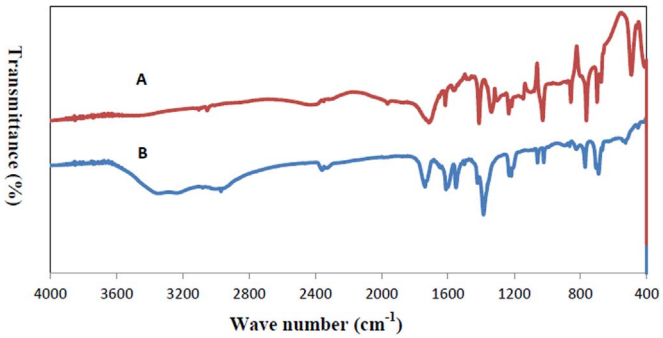

Fig. 1. FT-IR spectra of (A) isonicotinic acid and (B) 1.

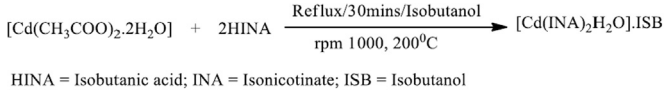

HINA = Isobutanic acid; INA = Isonicotinate; ISB = Isobutanol

Scheme 1. Synthetic method of 1.

the oxygen of the carboxylate and the nitrogen of the pyridine atom. The absorption band in the ~ 3351–3218 cm^{-1} assignable to νOH originating from coordinated H_2O and isobutanol molecule. The broadness is due to hydrogen bonding between oxygen of isobutanol and hydrogen of water [36]. The FT-IR spectra of the isonicotinic acid contain broad absorption band at 2610–2170 cm^{-1} attributed to the existence of O-H-N type of intermolecular hydrogen bonding. This band is completely absent in the compound confirming that the coordination is through the pyridine nitrogen and carboxylate oxygen atoms. The IR frequencies of vas(COO^-) and ν sym(COO^-) bands of the two carboxylate ligands coincide at 1546 and 1381 cm^{-1}, the difference Δ[Δ = vas(COO^-) – vs(COO^-) is 165 cm^{-1} indicating bidentate coordination modes of both carboxylate ligands [37]. Also, the absorption bands of the ν(C=O) that appeared in isonicotinic acid at 1742 cm^{-1} was observed to have been shifted to 1711 cm^{-1}, which also clearly indicates the coordination of the metal to isonicotinate through the carbonyl group (C=O). The ν(C-O) stretching band appeared at 1033 cm^{-1} in the ligand was shifted to 1014 cm^{-1} in **1** due to coordination. The ν(M-O) and ν(M-N) bands appeared as new bands at 527 and 441 cm^{-1} in the spectra of **1** [38]. The infrared spectra results are consistent with the results of the X-ray analysis.

3.2. UV–visible spectroscopy

The electronic spectra of ligand and **1** are shown in Figs. 2 and 3 respectively. The ligand has two bands at 250 nm and 289 nm which are assigned to π-π* and n-π*. These absorption bands were shifted to 221 nm and 261 nm (bathochromic shift) which may be due to complexation. As expected in Cd(II) of isonicotinic, there was no additional band in the visible region (d-d transition) [39].

3.3. Thermal studies

The thermal decomposition studies were carried out using TGA technique under N_2 atmosphere (Fig. 4). The thermal behavior of the compound was followed up to 600 °C. In the first stage of thermal decomposition, the compound starts to lose one isobutanol molecule between 50 and 110 °C (calculated 16.00%, experimental 16.10%) and then lost one molecule of coordinated water ~ 125 °C (calculated 4.03%, observed 4.10%) in the second stage. The third stage between 350 and 450 °C (calculated 55.15%, observed 58.0%) may be attributed to loss of two isonicotinic ligands. The three mass loss steps of the compound are in good agreement with the results of elemental analyses, infrared spectra and crystal structure of **1**.

3.4. BET

The surface area and porosity measurement of the **1** were determined volumetrically from N_2 adsorption (Fig. 5). The specific surface

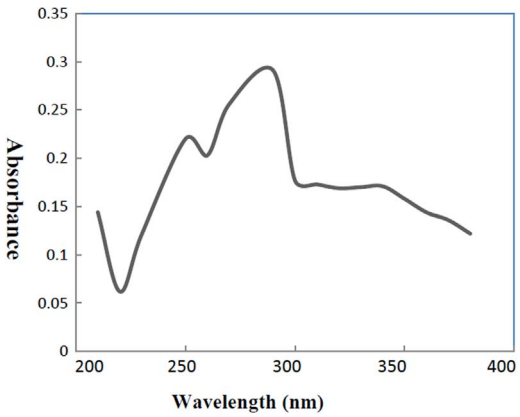

Fig. 2. UV–Vis spectra of ligand.

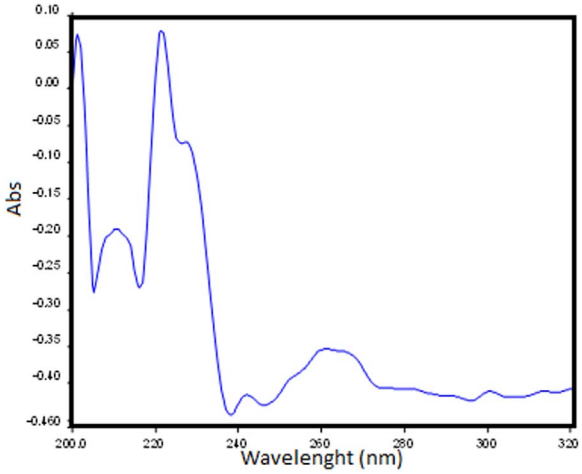

Fig. 3. UV–Vis spectra of 1.

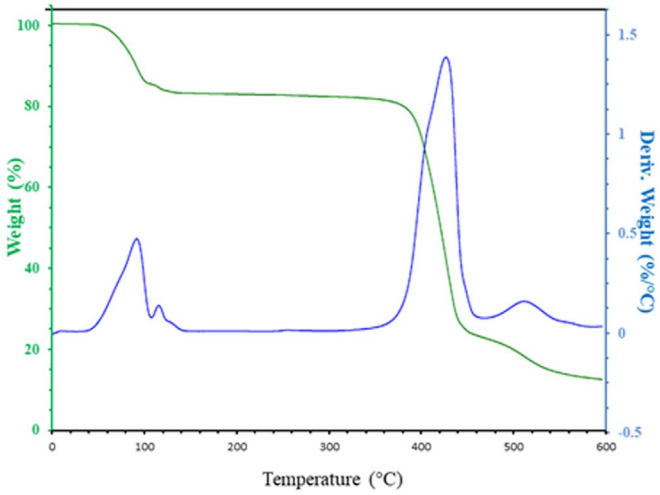

Fig. 4. The TGA profile in a nitrogen atmosphere for 1.

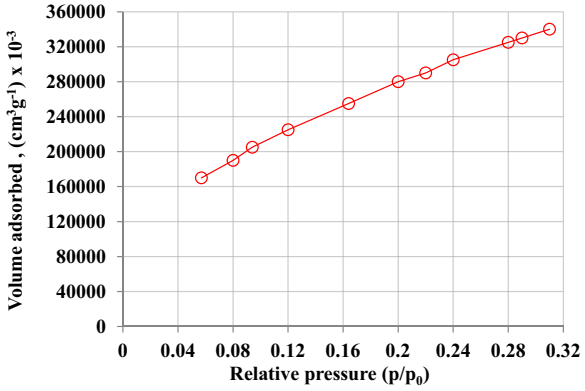

Fig. 5. Nitrogen isotherms of compound 1.

area of 1 based on the BET and Langmuir equation were calculated. The BET SSA is estimated to be 384 m^2g^{-1} (763 Langmuir). The pore volume and pore size were found to be 0.186 cm^3/g and 2.46 Å. It can be seen that **1** exhibited moderate surface area. MOFs possessing similar value of BET surface area have been reported [40,41].

3.5. Discussion on X-ray crystallography

The detailed crystallographic data and the structure refinement parameters are summarized in Table 1. Selected bond distances, angles

Table 1
Crystal data and structural refinement of $[Cd(INA)_2{\cdot}(H_2O)]$. ISB MOF.

Identification cypher	**$[Cd(INA)_2{\cdot}(H_2O)]$.ISB**
Empirical formula	$C_{12}H_{10}CdN_2O_5{\cdot}C_4H_7O$
Formula weight	445.72
Crystal system	Orthorhombic
Space group	*Pbca*
Crystal shape/color	Block/colorless
Unit cell dimensions	a = 12.2494(10) Å b = 15.4626(13) Å c = 18.8445(17) Å α = 90.00° β = 90.00° γ = 90.00°
Cell volume (Å^3)	3568.8
Z value	8
Density (calculated) (g cm^{-3})	1.659
F(000)	1783.994
Θ range for data collection	5–69°
Reflection measured/independent reflections	42,245/3311 (R_{int} = 0.037)
Cu Kα radiation,	λ = 1.54178 Å
Parameters/restraints	232/2
$wR(F^2)$	0.058
$R[F^2 > 2\sigma(F^2)]$	0.022

Table 2
Selected bond distances (Å) and angles (°) for 1.

Bond length (Å)		**Bond angles (°)**	
Cd1—N1	2.3488(14)	O1—Cd1—O2	53.73(4)
Cd1—N2	2.3904(16)	O1—Cd1—O3	139.74(4)
Cd1—O1	2.3428(13)	O1—Cd1—O4	86.14(4)
Cd1—O2	2.5330(12)	O1—Cd1—O5	88.08(5)
Cd1—O3	2.4345(12)	O1—Cd1—N1	136.68(4)
Cd1—O4	2.3976(12)	O1—Cd1—N2	89.72(5)
Cd1—O5	2.3055(13)	O2—Cd1—O4	139.72(5)
		O2—Cd1— N1	83.03(4)
		O2—Cd1—N2	89.72(5)
		O3—Cd1—N1	83.04(5)
		O3—Cd1—N2	87.74(4)

Table 3
Intermolecular interaction distances (Å) for 1.

D—H···A	**symm.**	**D—H**	**D···A**	**D—H···A**	**H···A**
O(5)-H(1)···O(2)	x − 1/2, y, − z + 3/2	0.81	2.02	2.829(3)	176(2)
O(5)-H(2)···O(6)	−	0.79	1.95	2.726(3)	170(3)
C(3)-H(31)···O(3)	− x + 1/2, y − 1/2, z	0.94	2.37	3.144(3)	139(1)
C(4)-H(41)···O(2)	− x + 1, y − 1/2, − z + 3/2	0.92	2.42	3.076(3)	129(1)
C(5)-H(51)···O(3)	− x + 1, y − 1/2, − z + 3/2	0.92	2.36	3.066(3)	134(1)
C(6)-H(61)···O(4)	x + 1/2, y, − z + 3/2	0.94	2.31	3.246(3)	176(1)
C(11)-H(111)··· O(3)	x − 1/2, − y + 1/2, − z + 1	0.95	2.39	3.081(3)	130(1)

and intermolecular interaction distances (Å) for **1** are given in Tables 2, 3. The Cd(II) is seven coordinate and exhibits an approximately pentagonal-pyramidal (CdN_2O_5) coordinate geometry. The ligand coordinates in a bidentate carboxylate mode (O, O^1).The Cd(II) atom is coordinated to four oxygen atoms in the equatorial plane (Cd1- O1 = 2.343, Cd1-O2 = 2.533, Cd1-O3 = 2.434, Cd1-O4 = 2.397 Å] from carboxylates, two nitrogen atoms in the axial position (Cd1-N1 = 2.390, Cd1- N2 = 2.349 Å) and one Oxygen atom Cd1-O5 = 2.306 Å from water molecule with isobutanol acting as counter ion. The average Cd-O bond length is 2.43 Å comparing favourably with the range 2.37–2.56 Å usually observed in Cd(II) compounds based on carboxylate with similar coordination mode [36–38,41–46]. The d (Cd1-N1 and d(Cd1-N2) are 2.3904(16) and 2.3488(14) respectively which are in agreement with the range (2.341–2.430 Å) reported for Cd(II) complexes with similar ligands. The Cd-Ow bond length [2.3055(13) Å] is similar and agreed with the value found for other seven coordinate cadmium (II) complexes [38,41] $[Cd(pth){\cdot}H_2O]$ where Pth = Pthalate ion [37], $[Cd(mal)(H_2O)_n]$ where mal^{2-} is malonate [37]. The C_4H_7O molecule found in the geometry coordinated outside the coordination sphere is linked by intermolecular hydrogen bond of the type O-H–O. The compound is stabilized by two hydrogen bonds namely intermolecular and intra molecular. The intramolecular hydrogen bonds are of the type C-H–O accounting for polymeric nature of **1**.

The Bond angles O1-Cd1-O4, O1-Cd1-N1, O1-Cd1-N2 and O2-Cd1-N2 are ranged between 87 and 92$^\theta$ near ideal 90$^\theta$ which are in accordance with results obtained for cadmium carboxylate complexes [45,46].

Based on the crystal structure of 1 as shown in Fig. 6, isobutanol as the guest molecule is bonded to Cd-Isonicotinate through intermolecular hydrogen bond. Crystal packing of compound **1** with open channels is depicted in Fig. 7.

The crystal compound was theoretically packed at point “a” and “c” to view the inclusion solvent within the crystal. Fig.s 7 and 8 clearly reflect isobutanol as the molecule trapped within the crystal pore. The calculated void volume is about 1007.89 A^3 per unit cell, which is about 28.2% of the total volume (Fig. 9).

3.6. Thermogravimetric analysis of 1d

Therrmogravimetric analysis of the **1d** (Fig. 10) yielded desolvated framework and shows a plateau in the temperature range from room temperature to 300 °C revealing that their pore channels were devoid of any guest molecules as shown in Fig. 10. Above this temperature the MOFs begins to decompose. The space originally occupied in **1** by the isobutanol guest molecule was left vacant after activation and the resulting material, **1d** is free from isobutanol guest molecule resulting into porous material.

3.7. Adsorption studies

1d was used for adsorption studies. The following physicochemical parameters such as initial concentrations of the adsorbent, contact time, temperature, adsorbent dosage and pH were varied to maximize the adsorption efficiency of the adsorbent on MO.

3.7.1. Effect of initial concentration

The effects of initial concentrations were studied at 25 ± 2 °C for 1 h using 0.01 g of adsorbent. Fig. S1 shows the amount of methyl orange adsorbed on **1** increased with increase in concentration up to 25 ppm and then started to decrease. The effect of the initial concentration factor depends on the immediate relation between the dye concentration and the available binding sites on an adsorbent surface [47]. The optimum concentration adsorbed was found to be 177.42 mg/g for **1** at a contact time of 1 h. For MO dye, the result implies that at low concentrations of the dye solutions, there still existed unoccupied adsorption sites that got occupied with increase in concentration [48]. At a 25 ppm when all the adsorption sites were saturated with dye molecules, the dye molecules started getting desorbed [49]. This accounts for the decrease in the amount of the dye molecules adsorbed at 30 mg/L for **1**. The increase in adsorption capacity with increasing methyl orange concentration could be due to higher probability of collision between the adsorbates molecule and the adsorbents surface [14,15].

3.7.2. Study on contact time

The effect of contact time was investigated at 25 ± 2 °C for the adsorption of methyl orange dye on **1** for 5 h and the plot of removal efficiency at different contact times is shown in Fig. S2. The methyl orange adsorption over **1** was rapid at the initial stages of the contact

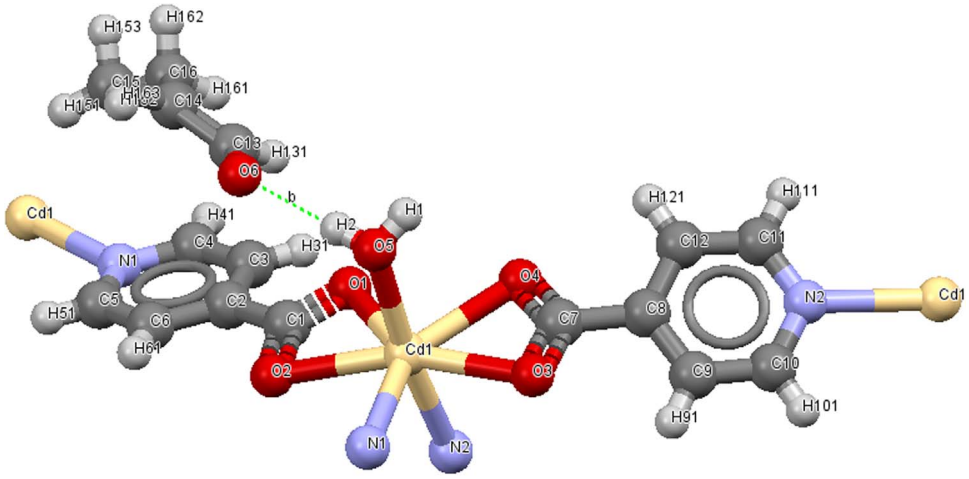

Fig. 6. Crystal structure of 1 with a view of coordination sphere of the cadmium cations with labeling and displacement ellipsoids drawn at the 50% probability level. Symmetry codes: (i) $x + 1/2, -y + 1/2, -z + 1$; (ii) $-x + 1, y + 1/2, -z + 3/2$; (iii) $-x + 1, y - 1/2, -z + 3/2$; (iv) $x - 1/2, -y + 1/2, -z + 1$.

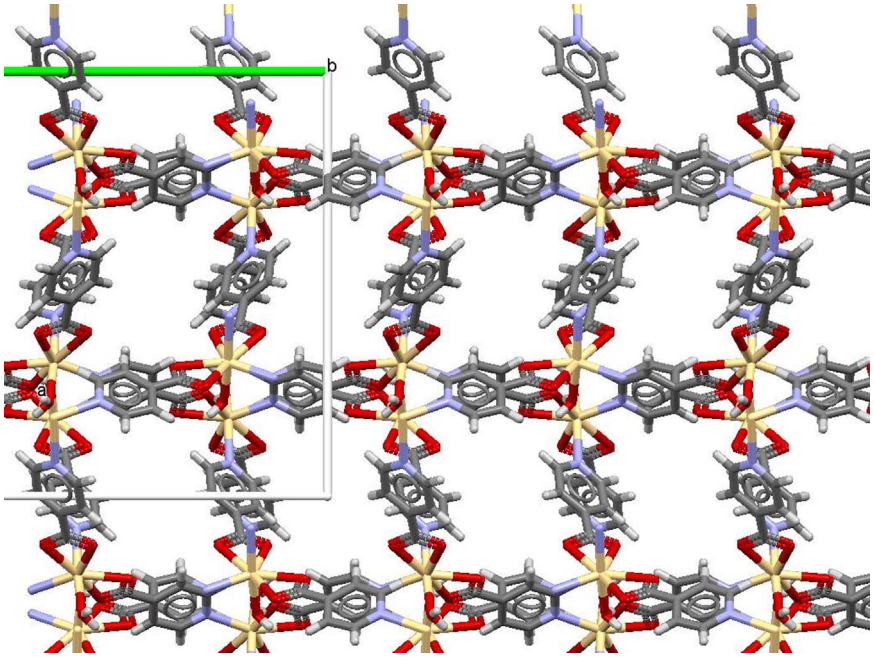

Fig. 7. 3D model view of 1 at point b revealing the empty space within the crystal lattice.

period, and thereafter it approached to equilibrium. This may be due to the presence of huge number of available vacant surface sites for adsorption during the initial stages of the adsorption [50,51]. As time passes, number of available vacant sites decreases and the adsorption sites become saturated. As shown in Fig. S2, the adsorbed quantity of methyl orange is high in **1** for the whole adsorption time. The adsorption over **1** is practically completed in 90 min and stability was maintain till 120 min, however, the adsorbed methyl orange increases slightly with increase in time up till 5 h.

3.7.3. Effect of temperature

The adsorption of dye is usually independent of the temperature of the solution [14,15,52,53]. However, the effect of temperature was studied using 0.01 g of adsorbent. Methyl orange adsorption over **1** was studied for a fixed time of 90 min at pH of 6.4. The temperature variation of adsorption of methyl orange dye over **1** was studied from 25 °C (room temperature) to 80 °C. Fig. S3 results reveal that the amounts of adsorbed methyl orange decrease as the temperature of the methyl orange solution increases. The maximum uptake of 188.71 mg/g was adsorbed at room temperature.

3.7.4. Effect of pH

Methyl orange dye adsorption over **1** was studied for a fixed time of 90 min at various pH values (from pH of 2 to pH of 12). The results of studies of pH effect as shown in Fig. S4, reveal that the amounts of adsorbed methyl orange is fairly high at pH of 7 and then continue to decrease with increasing pH. The maximum uptake of 181.29 mg/g was adsorbed at pH of 7 with **1** and thereafter, quantity adsorbed begins to decrease with further increase in the pH of the methyl orange solution.

3.7.5. Effect of adsorbent dosage

The results of studies of adsorbent dosage effect as shown in Fig. S5 reveal that the amounts of adsorbed methyl orange decrease rapidly with increase in the mass of the adsorbent. The maximum uptake of 168.06 mg/g was adsorbed when 0.01 g of **1** was used. The decrease in methyl orange uptake with increasing adsorbent dosage as shown in Fig. S1 may be due to complex interactions of several factors which might be due to insufficient availability of the methyl orange molecule to cover all the exchangeable sites on the MOF at high sorbent dosage, usually resulting to low methyl orange uptake [48,49]. Also, aggrega-

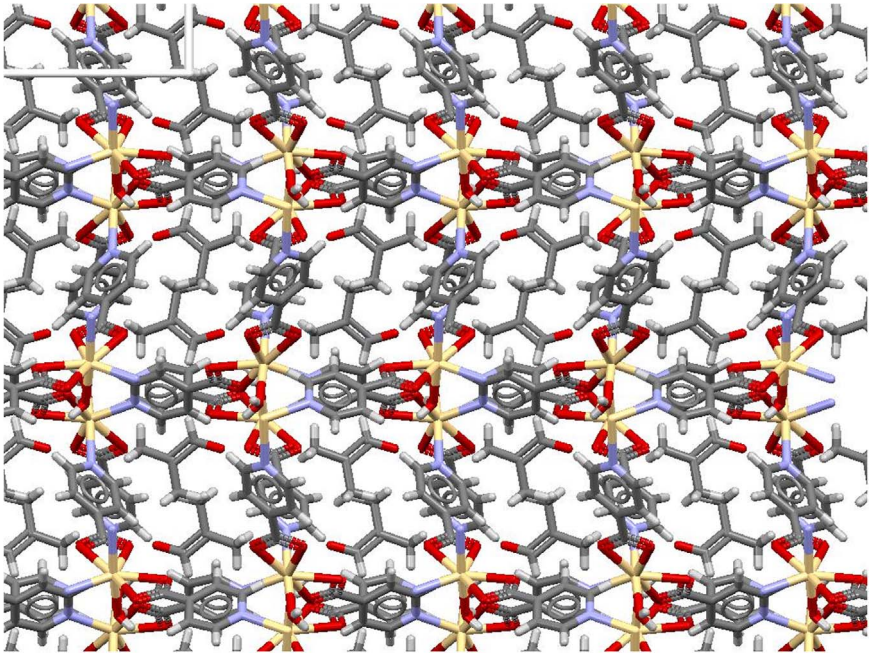

Fig. 8. 3D packing diagram of 1 reveals the open channels within the crystal lattice.

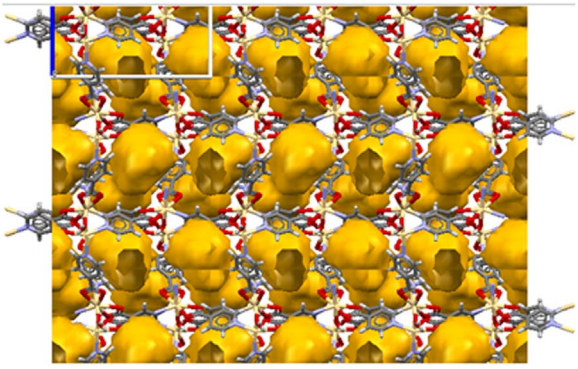

Fig. 9. 3D structure 1 model showing void space viewed at point a.

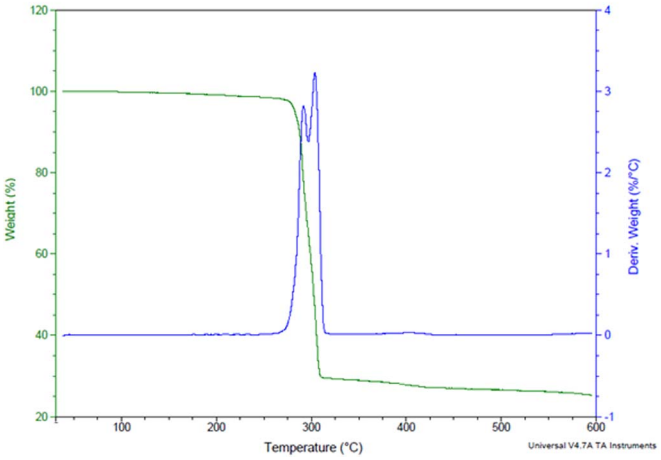

Fig. 10. Thermogravimetric analysis of 1d.

tion of sorbent particles at higher concentrations would lead to decrease in surface area and an increase in diffusion path length [51,54]. The unsaturation of the sorption sites during adsorption process might be another possibility as suggested by Gadd et al. [55].

3.7.6. Adsorption kinetic models

For the adsorption of Methyl orange on **1**, the pseudo-first order and pseudo-second order models were used to study the kinetics of the adsorption process. To compare the adsorption kinetics precisely, the adsorption data were first analyzed using the pseudo-first-order kinetic model [55].

$$\mathbf{log[qe - qt] = log[qe] - [k_1/2.303]t}$$

Therefore, the first order kinetic constant (k_1) can be calculated by $k_1 = -$ slope/2.303 when the log[qe − qt] is plotted against t. The plots of the pseudo-first-order kinetics of the dye adsorption over the **1** MOF at the initial concentration of 25 ppm are shown in Fig. S6 (adsorption time is only 0–5 h for good linearity and the kinetic constants are displayed in Table 4.Therefore, **1** is an effective adsorbent for Methyl orange removal in the viewpoint of adsorption amount and rate. Also for the adsorption of Methyl orange on **1**, the changes of adsorption amount with time are treated with the versatile pseudo-second-order kinetic model because the whole data during adsorption time can be treated successfully.

$$\mathbf{t/qt = 1/k_2q_e^2 + (1/q_e)t}$$

Where q_e: amount adsorbed at equilibrium (mg/g); q_t: amount adsorbed at time t(mg/g); t: adsorption time (h).

Therefore, the second-order kinetic constant (k_2) can be calculated by $k_2 = \text{slope}^2/\text{intercept}$ when the t/qt is plotted against t. The plots of the pseudo-second-order kinetics of the dye adsorption over the **1** at the initial concentration of 25 ppm are shown in Fig. S7. The calculated kinetic constants (k_2) and correlation coefficients (R^2) are shown in Table 4. Comparing the amount adsorbed at equilibrium, correlation coefficient and the linearity of the plot of the kinetics model for pseudo first order and pseudo second order, pseudo second order kinetics model is well favoured indicating the co-existence of physisorption and Chemisorption, with intra-particle diffusion being the rate controlling step for the adsorption of Methyl orange over **1**.

3.8. Adsorption isotherms

The sorption data have been subjected to different sorption isotherms, namely the Freundlich, Langmuir, Temkin and Dubinin-Radushevich isotherm.

Table 4
Adsorption kinetic parameters with coefficient of determination (R^2) for the adsorption of methyl orange over 1 at 25 ± 2 °C.

Adsorbent	Pseudo first order			Pseudo second order		
	k_1 $(min)^{-1}$	Q_e cal (mg g^{-1})	R^2	k_2 (g(mg $min)^{-1}$)	Q_e,cal (mg g^{-1})	R^2
$[Cd(INA)_2{\cdot}(H_2O)]$.ISB	2174.8	13.15	0.9129	200	0.00125	0.999

Table 5
Isotherm parameters with coefficient of determination (R^2) for the adsorption of methyl orange over $[Cd(INA)_2{\cdot}(H_2O)]$. ISB at 27 ± 2 °C.

MOFs	Langmuir isotherm			Freundlich isotherm			Temkin isotherm			D–R isotherm		
	Qm (mg/g)	K_L (L/mg)	R^2	Kf $(mg/g(L/mg)^{1/n})$	N	R^2	b_T	k_T (L/mg)	R^2	q_s (mg/g)	B_D (J/mol)	R^2
1	166.7	0.13	0.93	36.06	2.80	0.7	73.7	2.20	0.74	116.51	3×10^{-6}	0.85

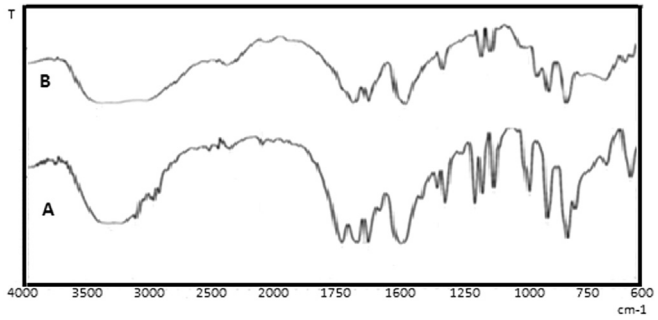

Fig. 11. FTIR spectra of (A) MO loaded 1 (B) 1.

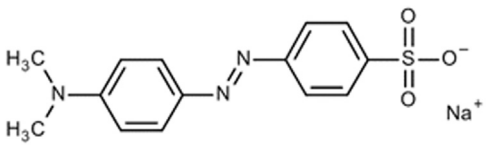

Fig. 12. Structure of methyl orange dye.

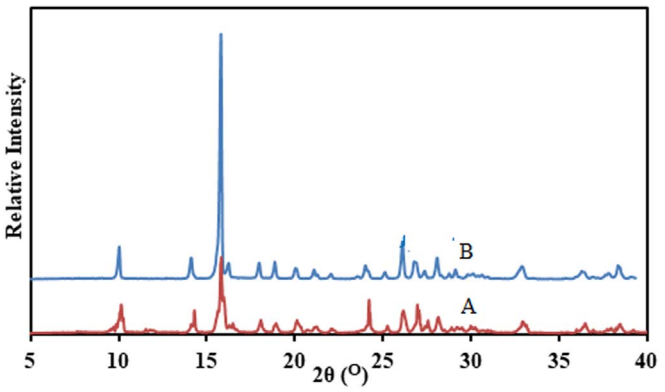

Fig. 13. X-ray powder diffraction of (A) MO loaded 1 (B) 1.

3.8.1. Langmuir isotherm

A linear plot was obtained when C_e/q_e was plotted against C_e over the entire concentration range of Methyl orange investigated, Fig. S8).

The Langmuir model described the sorption data with correlation coefficient of (R^2) 0.9319 values for **1**. The maximum sorption capacity (Q_m) and monomolecular capacity (KL) for **1** are found to be 167 mg/g and 0.130 L/g. The experimental data can be best described by the Langmuir isotherm model and revealed the ability of **1** to adsorb 167 mg of methyl orange per gram of adsorbent at 27 °C, pH 7.0 with adsorbent dosage of 0.130 g L^{-1}. The better fitting of the data (Fig. S8)

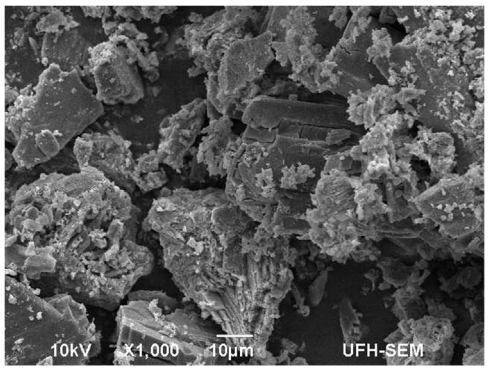

Fig. 14. Scanning Electron Micrograph of 1 before adsorption of MO dye.

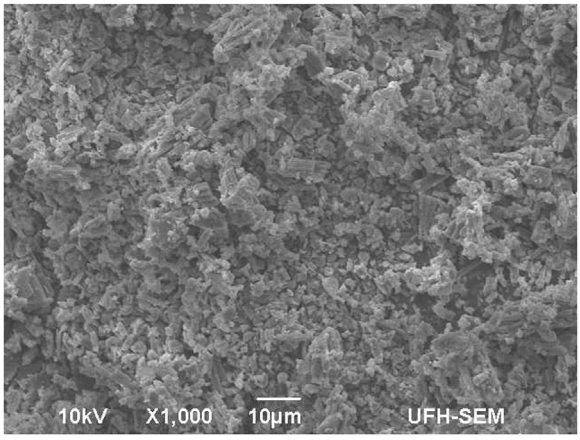

Fig. 15. Scanning Electron Micrograph of 1 after adsorption of MO dye.

shows that the adsorption of Methyl orange onto **1** is more of monolayer sorption rather than surface having heterogenous energy distribution [56].

From the slope and intercept of straight portion of the plot, the values of Freundlich parameters (Fig. S9), i.e., n and Kf are computed to be n = 2.801 and 36.06 for **1.** These values signify the sorption intensity and sorption capacity, respectively. The numerical value of n < 1 indicates that bound sorbate molecules interact in such a way that the binding strength is increased as more sorbate binds. Alternately, n > 1 can mean that sorption capacity is only slightly suppressed at lower equilibrium concentration and suggests multiple binding sites, with the highest strength sites binding the sorbate first [56–58]. The Freundlich sorption isotherm gives an expression encompassing the surface heterogeneity and the exponential distribution of active sites and their

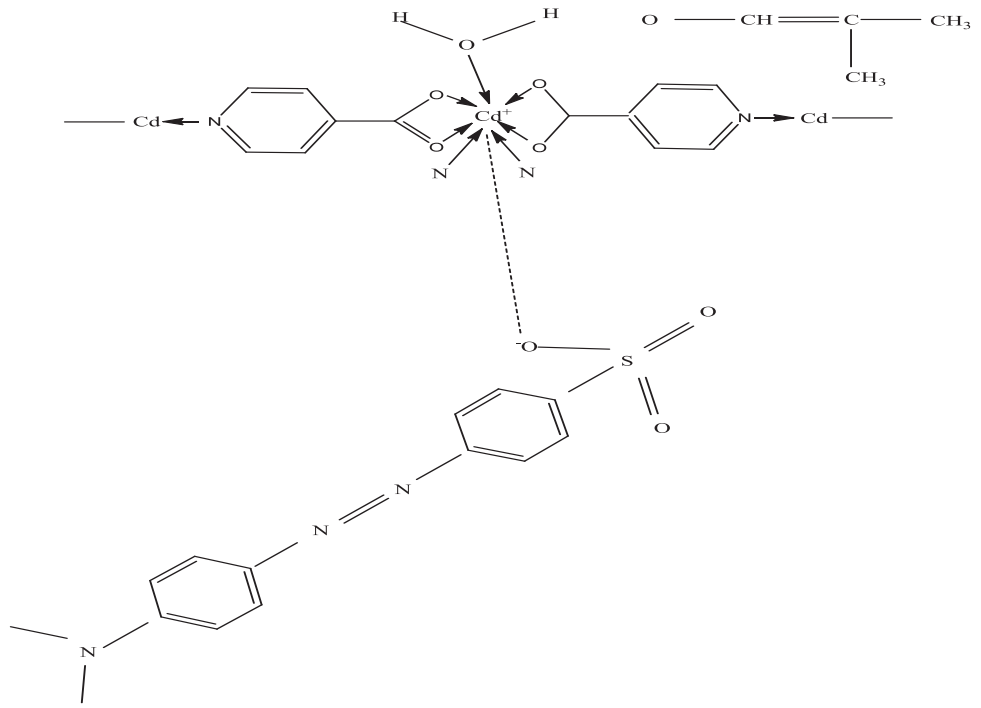

Fig. 16. Possible mechanism of adsorption of methyl-orange on 1.

energies. This isotherm does not predict any saturation of the sorbent by the sorbate, thus, infinite surface coverage is predicted mathematically, indicating a multilayer sorption of the surface [56].

3.8.2. Temkin isotherm

The Temkin parameters given in Table 5 were obtained by plotting q_e vs. In C_e. C_e is the equilibrium activities of dye and q_e is the surface activity for dye on the solid surface. The result was represented in Fig. S10.

3.8.3. Dubinin–Radushkevich isotherm

The parameters are given in Table 5. The type of adsorption of Methyl orange onto adsorbents is physical from the slope and intercept of this plot (Fig. S11). The values of $B_D = 3 \times 10^{-6}$ mol^2/kJ^2 and qs = 116.51 mgamd/g have been estimated for **1**. These values forecast the physical adsorption and chemical adsorption [57–59]. The regression coefficient values of Langmuir, Freundlich, Temkin and D–R models given in Table 5.0 indicated that Langmuir was the most suitable. The regression coefficient values R^2 show the applicability of the isotherms to the adsorption process. It can be seen from Figures 8.0 that Langmuir isotherm has the highest R^2 value of 0.93; therefore, it fits most to the adsorption process. The isotherms parameters are given in Table 5 below.

1 before and after adsorption removal of dye was characterized using Fourier infrared spectroscopy, scanning electron microscope and powder X-ray diffraction.

The results of infrared spectra of **1** (Table S3) before the removal of Methyl orange was compared with those obtained after the removal in the far IR region 4000–400 cm^{-1}. Fig. 11 shows the infrared spectra of the MOF before the removal was found to be different from those obtained after the removal and showed some new characteristic frequencies due to the adsorption of Methyl orange on the adsorbent [60].

The infrared spectrum showed that some peaks were shifted or disappeared and that new peaks were also detected. These changes observed in the spectrum indicated the possible involvement of those functional groups on the surface of **1**, during the adsorption process.

Extra bands at 1735, 1615, 1421 and 680 cm^{-1} were observed after adsorption of MO on 1

The strong band observed at 1056 cm^{-1} is associated to asymmetric stretches of S=O band in the adsorbent (Fig. 11, Table S3) which was not found in the structure of the adsorbent before adsorption [61]. This absorption band suggests adsorption of the MO (Fig. 12) onto **1**.

It can be seen from Fig. 13 that the diffraction peaks of MO loaded **1** were almost the same as that of the 1 which proves that the structure remains intact after adsorption. There was slight decrease in peak intensity due to decrease in crystallinity of the sample. Similar results have been reported for the adsorption of dyes onto different MOFs in literatures [62–64].

Scanning electron micrograph of **1** prior to its application clearly revealed that the crystals were porous in nature for adsorption to take place as observed in Fig. 14. Also, the scanning electron micrographs of **1** after adsorption of methyl orange (Fig. 15) depicted disappearance of pores indicating that the pores of the MOF have been filled with methyl orange dye.

3.8.4. Adsorption mechanisms

Methyl orange exists in negative forms, as anionic dye. The Adsorption of MO was studied in the pH range of 2–12 and it was discovered to pH dependent. Maximum adsorption occurred at pH 7.0 as shown in Fig. S4, This is due to the fact that MO dye in aqueous solution at a pH value of 7 exists in anionic form with negative charge on oxygen of SO_3^{2-}.

As shown in Fig. 16, **1** has positively charged Cd (II) sites with BET surface area of 384 m^2/g (Fig. 16), this might be small as to contain methyl orange dye molecule. Therefore, the only possible mechanism of methyl orange adsorption will be electrostatic interaction between the negatively charged dye molecule and the positively charged [Cd(INA)$_2$.ISB adsorbent. Similar adsorption mechanism of MO dye on MOFs via electrostatic interaction has been reported by many researchers [65–69].

It was observed that increase in pH from 7 to 12 resulted in decreases in amount of MO adsorbed which is in agreement with the previous reports [70,71]. When the pH is higher than 7, negative charged on the **1** increased and this does not favor adsorption of anionic dye due to electrostatic repulsion [69].

4. Conclusion

In this study, cadmium-based MOFs, [Cd $(INA)_2(H_2O)$].ISB **1** was synthesized and used for removal of methyl–orange from aqueous solution. **1** is pentagonal bipyramid (seven coordinate) around the cadmium (II) ion is of the form CdN_2O_5 coordinating to four oxygen atoms from carboxylates, one oxygen atom from water molecule and two nitrogen atoms of pyridine.

Adsorption process for **1** was found to favor the pseudo-first-order kinetics and the adsorption equilibrium data fitted best into the Langmuir isotherm. The adsorption capacity of the adsorbent for MO is 167 mg/g and the results suggest that the adsorption of methyl orange on the MOFs is partly due to electrostatic interaction between MO and the adsorbent. These findings reveal that **1** could be an effective adsorbent to remove methyl-orange from aqueous solution.

Supporting information available

CCDC 1039259 contains the supplementary crystallographic data for compound **1**. Copies of the data can be obtained free of charge at www.ccdc.cam.ac.uk/conts/retrieving.html or from the Cambridge Crystallographic Data Center, 12 Union Road, Cambridge CB2 1EZ, UK, Fax: + 44-1223-336-033; E-mail: deposit@ccdc.cam.ac.uk.

Appendix A. Supplementary material

Supplementary data associated with this article can be found in the online version at doi:10.1016/j.jssc.2017.07.019.

References

[1] C. Dey, T. Kundu, B.P. Biswal, A. Mallick, R. Banerjee, Crystalline metal-organic frameworks (MOFs): synthesis, structure and function, Acta Cryst. 870 (2014) 3–10.

[2] H.-L. Jiang, B. Liu, Y.-Q. Lan, K. Kuratani, T. Akita, H. Shioyama, F. Zhong, Q. Xu, From metal-organic framework to nanoporous carbon: toward a very high surface area and hydrogen uptake, J. Am. Chem. Soc. 133 (2011) 11854–11857.

[3] H.-C. Zhou, J.R. Long, O.M. Yaghi, Introduction to metal-organic frameworks, Chem. Rev. 112 (2012) 673–674.

[4] L.E. Kreno, K. Leong, O.K. Farha, M. Allendorf, R.P. Van Duyne, J.T. Hupp, Metal –organic framework materials as chemical sensors, Chem. Rev. 112 (2012) 1105–1125.

[5] H. Furukawa, K.E. Cordova, M. O'Keeffe, O.M. Yaghi, The Chemistry and applications of metal-organic frameworks, Science 341 (2013) 1230444.

[6] M. Li, D. Li, M. O ' Keefe, O.M. Yaghi, Topological analysis of metal-organic frameworks with polytopic linkage and/or multiple building units, Chem. Rev. 114 (2014) 1343–1370.

[7] K. Muller-Buschbaum, F. Beuerle, C. Feldman, MOF-based Luminescence tuning and chemical/physical sensing, Microporous Mesoporous Mater. 216 (2015) 171–199.

[8] D. Yan, B. Chen, Q. Duan, A copper-based metal-organic framework constructed from a new tetracarboxylic acid for selective gas separation, Inorg. Chem. Commun. 49 (2014) 34–36.

[9] J.-Q. Liu, J. Wu, F.-M. Li, W.-C. Liu, B.-H. Li, J. Wang, Q.-L. Li, R. Yadav, A. Kumar, Luminescent sensing from a new Zn(II) metal-organic framework, RSC Adv. 6 (2016) 31161–31166.

[10] J. Liu, G. Liu, C. Gu, W. Liu, J. Xu, B. Li, W. Wang, Rational synthesis of a novel 3,3,5-c polyhedral metal-organic framework with high thermal stability and hydrogen storage capability, J. Mater. Chem. A 4 (2016) 11630–11634.

[11] Y.-Q. Zhang, C.-C. Wang, X.-X. Guo, P. Wang, S.-J. Gao, Two 1D coordination polymers constructed from 3, 3o, 4, 4o biphenyltetracarboxylic acid and 4,4o-bipyridine: hydrothermal, syntheses and photocatalytic performance, Transit. Met. Chem. 41 (2016) 15–24.

[12] J. Liu, I. Chen, H. Cui, J. Zhang, L. Zhang, C.-Y. Su, Application of metal - organic frameworks in heterogeneous supramolecular catalysis, Chem. Soc. Rev. 43 (2014) 6011–6061.

[13] S. Qiu, M. Xue, G. Zhu, Metal-organic framework membranes: from synthesis to separation application, Chem. Soc. Rev. 43 (2014) 6116–6140.

[14] E. Haque, J. Lee, S.-H. Jung, I.-T. Jang, K.H. Young, C. Jong-San, J. Jonggeon, H.W. Sung, Adsorptive removal of methyl orange from aqueous solution with metal organic frameworks, porous chromium-benzenedicarboxylates, J. Hazard. Mater. 181 (2010) 535–542.

[15] E. Haque, W.J. Jong, H.J. Sung, Adsorptive removal of methyl orange and methylene blue from aqueous solution with a metal-organic framework material, iron terephthalate (MOF-235), J. Hazard. Mater. 185 (2011) 507–511.

[16] D.J. Trenchemontaane, J.L. Mendoza-Cortes, M. O'Keeffe, O.M. Yaghi, Secondary building units, nets and bonding in the chemistry of metal-organic frameworks, Chem. Soc. Rev. 378 (2009) 1257–1283.

[17] A.C. Tella, I.Y. Aaron, Syntheses and applications of metal-organic frameworks materials: a review, Acta Chim. Pharm. Indic. 2 (2) (2012) 75–81.

[18] D.J. Tranchemontagne, J.R. Hunt, O.M. Yaghi, Room temperature synthesis of metal-organic frameworks: MOF-5, MOF-74, MOF-177, MOF-199, and IRMOF-0, Tetrahedron 64 (2008) 8553–8557.

[19] D. Zacher, O. Shekhah, C. Woll, R.A. Fischer, Thin films of metal-organic frameworks, Chem. Soc. Rev. 38 (5) (2009) 1418–1429.

[20] A.A. Filipe, K. Jacek, Hydrothermal synthesis and structural characterization of a novel cadmium-organic framework, J. Solid State Chem. 177 (2004) 3423–3432.

[21] D. Chandan, K. Tanay, P.B. Bishnu, M. Arijit, B. Rahul, Crystalline metal-organic frameworks (MOFs): synthesis, structure and function, Acta Cryst. B70 (2014) 3–10.

[22] Y.K. Seo, G. Hundal, I.T. Jang, Y.K. Hwang, C.H. Jun, J.S. Chang, Microwave synthesis of hybrid inorganic–organic materials including porous $Cu_3(BTC)_2$ from Cu(II)-trimesate mixture, Microporous Mesoporous Mater. 119 (2009) 331.

[23] C.G. Carson, A.J. Brown, D.S. Sholl, S. Nair, Sonochemical synthesis and characterization of submicrometer crystals of the metal-organic framework Cu (hfipbb)(H(2)hfipbb)(0.5), Cryst. Growth Des. 11 (2011) 4505–4510.

[24] M.I. Florez-Zamora, Comparative study of Al-Ni-Mo alloys obtained by mechanical alloying in different ball mills, Rev. Adv. Mater. Sci. 18 (2008) 301.

[25] A.C. Tella, O.A. Ameen, P.A. Ajibade, L.O. Alimi, Template metal-organic frameworks: solvent- free synthesis, characterization and powder X-ray diffraction studies of $[Cu(NO_3)2(bipy)2](py)_2$, J. Porous Mater. 22 (5) (2015) 1599–1605.

[26] A.C. Tella, S.O. Owalude, A Green route approach to synthesis of Ni(II) and Zn(II) templated metal-organic frameworks, J. Mater. Sci. 49 (2014) 5635–5639.

[27] A. Hijazi, A. Mcheik, H. Rammal, W. Rammal, A. Houssein, J. Toufaily, T. Hamieh, Biosorption of methylene blue from waste water using *Lebanese Cymbopogon citratus (citronnelle)*, Eur. Sci. J. 11 (21) (2015) 293–307.

[28] T. Robinson, G. MuMullan, R. Marchant, P. Nigam, Remediation of dyes in textile effluent: a critical review on current treatment technologies with a proposed alternative, Bioresour. Technol. 77 (2000) 247–255.

[29] V.K. Gupta, R. Kumar, A. Nayak, T.A. Saleh, M.A. Barakat, Adsorptive removal of dyes from aqueous solution onto carbon nanotubes: a review, Adv. Colloid Interface Sci. 193–194 (2013) 24–43.

[30] D.V. Patil, P.B.S. Rallapalli, G.P. Danji, R.J. Tayade, R.S. Somani, H.C. Raji, MIL-53(Al): an efficient adsorbent for the removal of nitrobenzene from aqueous solution, Ind. Eng. Chem. Res. 50 (2011) 10516–10524.

[31] Y. Wu, G. Xu, W. Liu, J. Yang, F. Wei, L. Li, W. Zhang, Q. Hu, Postsynthetic modifications of copper terephthalate metal-organic frameworks and their new applications in preparation of samples containing heavy metal ions, Microporous Mesoporous Mater. 210 (2015) 110–115.

[32] A.C. Tella, S.O. Owalude, C.A. Ojekanmi, S.O. Oluwafemi, Synthesis of copper–isonicotinate metal–organic frameworks simply by mixing solid reactants and investigation of their adsorptive properties for the removal of the fluorescein dye, New J. Chem. 38 (2014) 4494–4500.

[33] A.C. Tella, S.O. Owalude, S.J. Olatunji, V.O. Adimula, S.E. Elaigwu, L.O. Alimi, P.A. Ajibade, O. Oluwafemi, Synthesis of zinc-carboxylate metal-organic framework for the removal of emerging drug contaminant (Amodiaquine) from aqueous solution, J. Environ. Sci. (2017). http://dx.doi.org/10.1016/j.jes.2017.06.015.

[34] G.M. Shelderick, SHELX-97. Programme for Crystal Structure Refinement, University of Gottingen, Germany, 1997.

[35] K.-Y.A. Lin, S.-Y. Chen, A.P. Jochems, Zirconium-based metal organic frameworks: highly selective adsorbents for removal of phosphate from water and urine, Mater. Chem. Phys. 160 (2015) 168–175.

[36] K. Nakamoto, Infrared and Raman Spectra of Inorganic and Coordination Compounds, 3rd edition, John Wiley, New York, 1978.

[37] B. Barszcz, J. Masternak, M. Hodorowicz, A. Jablonska-Wawrzycka, Cadmium(II) and Calcium(II) complexes with *N,O*-bidentate ligands derived from pyrazinecarboxylic acid, J. Therm. Anal. Calorim. 108 (2012) 971–978.

[38] O.R. Evans, R.-G. Xiong, Z. Wang, G.K. Wong, W. Lin, Crystal engineering of acentric diamondoid metal-organic coordination networks, Angew. Chem. Int. Ed. 38 (4) (1999) 536–538.

[39] A.C. Tella, J.A. Obaleye, Divalent metal complexes of 4-amino-N-pyrimidin-2-yl benzene sulphonamide and their antimalarial activities against *plasmodium berghei*, Bull. Chem. Soc. Ethiop. 25 (3) (2011) 371–380.

[40] N. Getachew, Y. Chebule, I. Diaz, M. Sanchez – Sanchez, Room temperature synthesis of metal-organic framework MOF-2, J. Porous Mater. 21 (5) (2014) 769–773.

[41] A. Phan, A.U. Czaja, F. Gandara, C.B. Knobler, O.M. Yaghi, Metal-organic frameworks of vanadium as catalysts for conversion of methane to acetic acid, Inorg. Chem. 50 (2011) 7388–7390.

[42] T.C. Stamatatos, K. Katsoulakou, V. Nastopoulos, C.P. Raptopoulou, E. Manessi-Zoupa, S.P. Perlepes, Cadmium carboxylate chemistry: preparation, crystal structure, and thermal and spectroscopic characterization of the one-dimensional polymer$[Cd(O_2CMe)(O_2CPh)(H_2O)_2]_n$, Z. Nat. 58b (2003) 1045–1054.

[43] J.L.L. Vaz, G. Duc, M. Petit-Ramel, R. Faure, O. Vittori, Cd(II) complexes with phthalic acid: solution study and crystal structure of Cadmium(II) phthalate hydrate, Can. J. Chem. 74 (1996) 359–364.

[44] S. Banerjee, P.-G. Lassahn, C. Janiak, A. Ghosh, Supramolecular architecture of Cadmium(II)-terephthalate complexes having a tridentate or tetradentate Schiff base as blocking coligand, Polyhedron 24 (2005) 2963–2971.

[45] V. Aletras, N. Hadjiliadis, D. Stabaki, A. Karaliota, M. Kamariotaki, I. Butler, J.C. Plakatouras, S. Perlepes, Preparation and characterization of the seven coordinate cadmium(II) complex $[Cd(3,4\text{-}H_2dhb)_2(H_2O)_3]\cdot HCl\cdot(3,4\text{-}H_3dhb)\cdot$

2.5H_2O; the first structural determination of a complex containing the 3,4-dihydroxybenzoato(-1)(3,4-H_2dhb^-) ligand, Polyhedron 16 (8) (1997) 1399–1402.
[46] F. Jian, H. Xiao, P. Sun, P. Zhao, Crystal structure and characterization of the Dinuclear Cd(II) complex $[Cd(H_2O)_2(o\text{-}HOC_6H_4COO)_2]_2$, Molecules 9 (2004) 876–882.
[47] J.-R. Li, R.J. Kuppler, H.C. Zhou, Selective gas adsorption and separation in metal–organic frameworks, Chem. Soc. Rev. 38 (2009) 1477.
[48] P.-Y. Du, H. Li, X. Fu, W. Gu, X. Liu, A 1D anionic lanthanide coordination polymer as an adsorbent material for the selective uptake of cationic dyes from aqueous solution, Dalton Trans. 44 (2015) 13752–13759.
[49] A. Mittal, A. Malviya, D. Kaur, J. Mittal, L. Kurup, Studies on the adsorption kinetics and isotherms for the removal and recovery of methyl-orange from waste waters using waste materials, J. Hazard. Mater. 148 (2007) 229–240.
[50] G. Ferey, Hybrid porous solids: past, present, future, Chem. Soc. Rev. 37 (2008) 191.
[51] M.J. Martin, A. Artola, M.D. Balaguer, M. Rigola, Activated carbons developed from surplus sewage sludge for the removal of dyes from dilute aqueous solution, Chem. Eng. J. 94 (2003) 231–239.
[52] M.Y. Masoomi, A. Morsali, P.C. Junk, Rapid mechanochemical synthesis of two new Cd(II)-based MOFs with high removal efficiency of Congo red, CrystEngComm 17 (2015) 686–692.
[53] E.R. Garcia, R.L. Medina, M.M. Lazano, I.H. Perez, M.J. Valero, A.M.M. Franco, Adsorption of Azo-dye orange II from aqueous solution using a metal-organic framework material: iron-benzenetricarboxylate, Materials 7 (12) (2014) 8037–8057.
[54] G.M. Gadd, C. White, L. De- Rome, Heavy metal and radionuclide uptake by fungi and yeasts, in: P.R. Norris, D.P. Kelly (Eds.), Biohydrometallurgy, A. Rowe, Chippenham Wilts, UK, 1988.
[55] M.S. Chiou, H.Y. Li, Equilibrium and kinetic modeling of adsorption of reactive dye on cross-linked chitosan beads, J. Hazard. Mater. 93 (2002) 233–248.
[56] E. Haque, J.W. Jun, S.H. Jhung, Adsorptive removal of methyl orange and methylene blue from aqueous solution with a metal-organic framework material, iron terephthalate (MOF-235), J. Hazard. Mater. 185 (2011) 507–511.
[57] S.M. Hasany, M.M. Saeed, M. Ahmed, Sorption and thermodynamic behavior of zinc (II)-thiocyanate complexes onto polyurethane foam from acidic solutions, J. Radioanal., Nucl., Chem. 252 (2002) 477–484.
[58] M. Saleem, M. Afzal, R. Qadeer, J. Hanif, Selective adsorption of uranium on activated-charcoal from electrolytic aqueous solutions, Sep. Sci. Technol. 27 (2) (1992) 239–253.
[59] M. McGoff, Design of Crystalline Solids via Solid State Reaction (B.Sc. Thesis Submitted), Worcester Polytechnic Institute, USA, 2008.
[60] L. Ai, C. Zhang, L. Meng, Adsorption of methyl orange from aqueous solution on hydrothermal synthesized Mg-Al layered double hydroxide, J. Chem. Eng. Data 56 (11) (2011) 4217–4225.
[61] M. Arshadi, F. SalimiVahid, J.W.L. Salvacion, M. Soleymanzadeh, Adsorption studies of methylorange on an immobilized Mn-nanoparticle: kinetic and thermodynamic, RSC Adv. 4 (2014) 16005–16017.
[62] Z. Zhang, A.S. Biradar, S. Pramanik, T.J. Emge, T. Asefa, J. Li, A new layered metal-organic framework as a promising heterogenous catalyst for olefin epoxidation reactions, Chem. Commun. 48 (2012) 6541–6543.
[63] K.-D. Zhang, F.-C. Tsai, N. Ma, Y. Xia, H.-L. Liu, X.-Q. Zhang, X.-Y. Yu, X.-Z. Zheng, T. Jiang, D. Shi, C.-J. Chang, Adsorption behavior of high stable Zr-based MOFs for the removal of acid organic dye from water, Materials 10 (205) (2017) 1–11.
[64] Z. Shi, L. Li, Y. Xiao, Y. Wang, K. Sun, H. Wang, L. Liu, Synthesis of mixed-ligand Cu-MOFs and their adsorption of malachite green, RSC Adv. 7 (2017) 30904–30910.
[65] Z.-H. Zhang, J.-L. Zhang, J.-M. Liu, Z.-H. Xiong, X. Chen, Selective and competitive adsorption of Azo dyes on metal-organic framework ZIF-67, Water Air Soil Pollut. 227 (2016) 471.
[66] C. Jiang, B. Fu, H. Cai, T. Cai, Efficient adsorptive removal of congo red from aqueous solution by synthesized zeolite imidazolate framework-8, Chem. Speciat. Bioavailab. 28 (1–4) (2016) 199–208.
[67] B.K. Jung, J.W. Jun, Z. Hasan, S.H. Jsung, Adsorptive removal of p-arsanilic acid from water using mesoporous zeolitic imidazolate framework-8, Chem. Eng. J. 267 (2015) 9–15.
[68] X. Yan, X. Hu, T. Chen, S. Zhan, M. Zhou, Adsorptive removal of 1-napthol from water with zeolitic imidazole framework-67, J. Phys. Chem. Solids 107 (2017) 50–54.
[69] B.K. Jung, Z. Hasan, S.H. Jhung, Adsorptive removal of 2,4- dichlorophenoxyacetic acid (2,4-D) from water with a metal- organic framework, Chem. Eng. J. 234 (2013) 99–105.
[70] L. Wang, A. Wang, Adsorption properties of congo red from aqueous solution onto surfactant-modified montmorillonite, J. Hazard. Mater. 160 (2008) 173–180.
[71] C. Leodopoulos, D. Doulia, K. Gimouhopoulos, T.M. Triantis, Single and simultaneous adsorption of methyl orange and Humic acid onto betonite, Appl. Clay Sci. 70 (2012) 84–90.